Hindawi Publishing Corporation
Texture, Stress, and Microstructure
Volume 2010, Article ID 910793, 10 pages
doi:10.1155/2010/910793

Research Article

Thermal and Electric Field-Dependent Evolution of Domain Structures in Polycrystalline $BaTiO_3$ Using the 3D-XRD Technique

Mesut Varlioglu,[1] Ulrich Lienert,[2] Jun-Sang Park,[3] Jacob L. Jones,[4] and Ersan Üstündag[1]

[1] *Materials Science and Engineering, Iowa State University, Ames, IA 50011, USA*
[2] *Advanced Photon Source, Argonne National Laboratory, Argonne, IL 60439, USA*
[3] *Sibley School of Mechanical and Aerospace Engineering, Cornell University, Ithaca, NY 14853, USA*
[4] *Materials Science and Engineering, University of Florida, Gainesville, FL 32611, USA*

Correspondence should be addressed to Ulrich Lienert, lienert@aps.anl.gov

Received 23 June 2010; Accepted 1 October 2010

Academic Editor: Adam Morawiec

The evolution of ferroelectric domain structures inside a single grain embedded in a polycrystalline BaTiO3 ceramic was investigated under temperature and electric field using the three-dimensional X-ray diffraction (3D-XRD) method. The orientation of domains within the grain was studied during the phase transformation from the cubic to tetragonal crystal structure. The peak widths broadened from $0.10 \pm 0.01^\circ$ to $0.29 \pm 0.08^\circ$ along the azimuthal direction during cooling. Four individual tetragonal domain structures were developed from the cubic grain. A twinning model based on {101} habit planes is discussed. While the twinning model predicts 89.47° misorientation between 90° domains and 1.049° misorientation between domain variants, the measured misorientations neither support the twinning model nor are the domain structures mutually orthogonal. The average misorientation of the domain structures at room temperature with respect to the cubic grain was about 0.3°. Upon application of an electric field, the volume fractions of the domain structures changed systematically favoring growth of domain structures with small polarization angle with respect to applied field direction. No rotation of domain structures was observed upon application of an electric field which is consistent with domain boundary migration.

1. Introduction

Ferroelectric ceramics have been widely used in microelectronic and sensing applications because of their ability to convert mechanical energy into electrical energy and *vice versa* [1]. Since the discovery of ferroelectricity, $BaTiO_3$ has been one of the most widely investigated ferroelectrics because of its relatively simple and chemically stable crystal structure [2–4]. When $BaTiO_3$ is cooled from a temperature above the Curie temperature to room temperature, the paraelectric cubic phase (space group: Pm $\bar{3}$ m) transforms to ferroelectric tetragonal (space group: P4 mm) structure. This phase transformation creates a large stress due to the deviatoric and volumetric transformation strains and a spontaneous polarization is developed parallel to the cubic ⟨100⟩ directions to minimize the energy of the system [5]. The regions of the unit cells that orient along a uniform direction are called domains, and populations of the ferroelectric domains in a grain with a distinct orientation are called domain structures. The final microstructure of tetragonal $BaTiO_3$ is composed of 90° and 180° domain structures where the polarization vectors of adjacent domains are approximately perpendicular or parallel to each other, respectively. The angle between the c-axes of two domains separated by a 90° domain wall is given by γ, which is related to the lattice aspect ratio of c/a through

$$\gamma = 2\tan^{-1}\left(\frac{a}{c}\right). \tag{1}$$

For example, $\gamma = 89.47^\circ$ for polycrystalline $BaTiO_3$ with $c/a = 1.0092$. Therefore, the angle between a and c axes of two adjacent domains is 0.53°.

Ferroelectric materials are widely produced with conventional ceramic processing techniques [2] in polycrystalline form. The microstructure is composed of grains with distinct orientations, and each grain contains domains that are oriented with respect to each other by specific symmetry operations. With the application of an electric field or a mechanical load, ferroelectric (ferroelastic) domain volumes tend to change via domain wall motion. For instance, compressive loads create a preference of the ferroelastic domains aligned with their *c*-axis in a plane normal to the compression axis. Likewise, electric fields create a preference for domains to align with their *c*-axis parallel to the electric field. Domain reorientation in one grain generally results in a change in local stress state and electrical state in the neighboring grains, leading to additional boundary constraints on the original grain. While ferroelectrics are often characterized using techniques that average the response of grain orientations (e.g., X-ray and neutron powder diffraction), quantification of the local ferroelectric constitutive behavior such as the internal strain and domain switching at the inter- and intragranular level requires a different approach. Several techniques such as transmission electron microscopy (TEM) [6, 7], white beam topography [8], electron backscatter diffraction (EBSD) [9], optical microscopy, and atomic force microscopy [10, 11] have been used to characterize the ferroelectric domain structure under thermo-electro-mechanical conditions. However, low penetration depth of these characterization techniques prevents a study on the orientation, strain, and mesoscale dynamics of the domains embedded inside the polycrystalline ferroelectrics.

The three-dimensional X-ray diffraction (3D-XRD) technique [12, 13] is a recently developed synchrotron method that offers unique opportunities to study the mesoscale response of polycrystalline materials in response to external stimuli such as mechanical or electrical load. The 3D-XRD method utilizes monochromatic high-energy X-rays that may be microfocused (as small as $5 \times 5\,\mu m^2$) to a desired location on the sample while oscillating the sample on a rotation stage. This technique makes it possible to study the three-dimensional orientation structure of individual grains embedded in a polycrystal as well as the position, volume, orientation, and elastic strain of those individual grains [14]. To measure the *in situ* electromechanical response of ferroelectric domains embedded in a grain, a polycrystalline $BaTiO_3$ sample was subjected to an electric field during 3D-XRD measurements in this work.

2. Experimental Procedure

A polycrystalline $BaTiO_3$ ceramic was processed using conventional high-temperature sintering [15] of $BaTiO_3$ powder (of 99.9% purity, with Ba/Ti ratio = 1.0, Ferro Corp., Transelco Division). The nominal grain size was measured as approximately 20 μm in an independent electron backscatter diffraction (EBSD) study. The samples were sectioned using a diamond saw, and their surfaces were polished with abrasive paper until the final dimensions were approximately $1 \times 1 \times 5\,mm^3$. Two parallel $1 \times 5\,mm^2$ surfaces were sputter-coated with gold, then thin copper wires were attached on them using a conductive epoxy. These sample dimensions were chosen because they offer several advantages: the high-energy X-rays (80.72 keV in the present study) can easily penetrate through 1 mm thickness and the applied electric field is sufficiently higher than the coercive field and yet lower than the dielectric-breakdown strength of the material.

The 3D-XRD experiments of $BaTiO_3$ were performed at beamline 1-ID-C of the Advanced Photon Source (APS), Argonne National Laboratory, Argonne, IL. This beamline provides dedicated high-energy focusing optics and is specialized for 3D-XRD data acquisition and analysis. By focusing vertically and using the horizontal slits, high-energy X-rays (energy = 80.72 keV) in transmission mode were focused to a $20 \times 20\,\mu m^2$ spot size. The sample was centered on a rotation stage with vertical rotation axis. The setup is sketched in Figure 1. The sample-to-detector distance was measured as 2274.3 mm using a Ceria (CeO_2) calibration powder. This large distance enhanced the resolution of the diffraction spots on the GE 41RT amorphous silicon detector [16] (which has 2048×2048 pixels, 200 μm pixel size from GE Healthcare, Inc.) and thus increased the radial angle resolutions of the variants of {001}, {011}, {111}, {002}, {012}, and {112} diffraction planes. To heat the $BaTiO_3$ sample, a Thunderbolt electric cartridge heater (Vulcan Electric Co. Model: TB3815A) was used. This device is embedded in the sample holder which was made of copper for high thermal conductivity. An electrically insulating but heat-conductive epoxy was applied between the sample and the sample holder to prevent electric arcing. The temperature profiles of the copper plate and sample were measured using thermocouples and an Inframetrics Model 760 IR imaging radiometer. The temperature outputs from thermocouples were monitored using an Omega model HH21 thermometer and Fluke 87IV true RMS multimeter. To prevent heating the position stage while heating the sample, MACOR machinable glass ceramic posts were used to separate the sample stage from the positioning stage.

Prior to applying the electric field, the sample was heated to a temperature above the Curie temperature to ensure that the domains inside the sample were initially randomly oriented. Diffraction patterns were collected by exposing the detector while oscillating the sample in 0.25° steps about the ϕ axis, covering a total range of ±60°. After cooling, the data collection procedure was repeated at each applied electric field within the same ϕ range. The electric field was applied *in situ* using a Canberra 3002 HV supply with 5 and 10 kV/cm steps. The direction of the electric field remained constant with respect to the sample coordinate system (along the *y*-axis at $\phi = 0°$ and rotates with the sample as seen in Figure 1). The maximum applied electric field was high enough to cause domain reorientation as the nominal coercive field of the material was previously measured as 5.16 kV/cm [17].

The diffraction patterns collected above the Curie temperature were indexed using the GRAINDEX indexing software [12, 18]. At 130°C, sharp and nonsplitting peaks were observed belonging to a cubic structure. A grain with high completeness was selected as reference grain. Because the beam width was much smaller than the sample thickness, this grain must be close to the rotation axis and is therefore

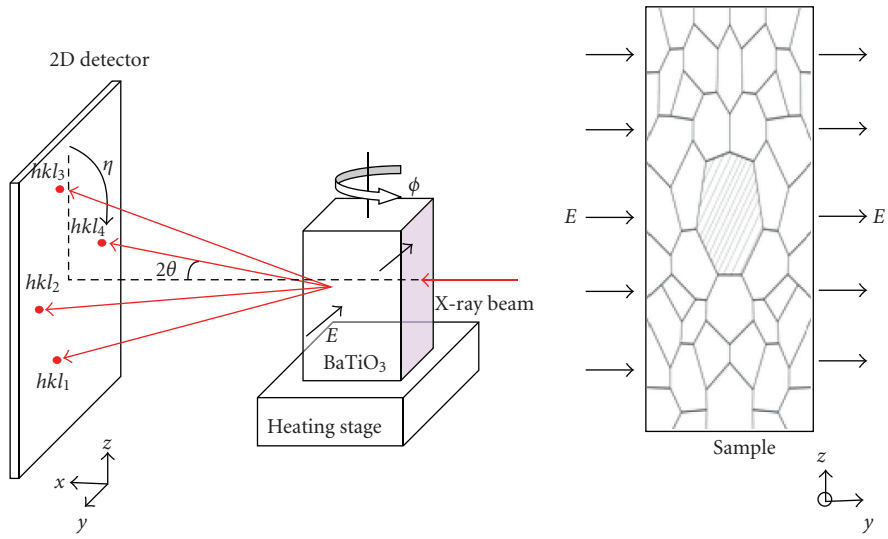

Figure 1: (a) Schematic representation of the 3D-XRD setup used on beamline 1-ID-C at the Advanced Photon Source (APS), in Argonne National Laboratory. (b) A view along the X-ray beam (parallel to the x axis) at $\phi = 0°$. The electric field direction was roughly parallel to the y axis at $\phi = 0°$.

a bulk grain. During the experiment setup, full illumination of the reference grain was verified by moving the X-ray beam in horizontal and vertical directions (Y and Z direction in Figure 1). X-ray patterns recorded for sample translations by $\pm 20\,\mu$m showed no evidence of reflections from the reference grain. Considering that the full grain was illuminated with X-rays, we observed the sum of the diffraction from all reflecting domains. The same grain was tracked while cooling the sample to room temperature and applying the electric field. Since domain structures diffract as a population within 0.6° of ϕ, the ROI images of each peak were obtained from integrating all diffraction patterns recorded at $\pm 0.5°$ ϕ range with respect to initial ϕ location of the cubic reflection and observing the changes in the cubic reflections when cooling to room temperature. It was also verified that the grain was fully illuminated by the incident X-ray beam by the observation that increasing the beam size did not increase the diffracted intensities.

In order to measure the orientations of the grains with GRAINDEX, a set of parameters including the experiment setup and crystallographic parameters of the sample have to be known. While experiment setup parameters were verified with calibration tools, crystallographic parameters were calculated from the sample itself. To measure the overall lattice parameters of polycrystalline $BaTiO_3$ sample at both phases, complete Debye-Scherrer rings were obtained by summing diffraction images taken within ±60° of ϕ and ±180° of η using the *Fit2D.v12.077* software [19]. Each diffraction peak corresponding to a diffraction plane was least-squares fitted using a Gaussian profile shape function using MATLAB (Ver. 7.0.4, MathWorks, Inc.). The lattice parameters at each phase were calculated by using Cohen's method [20]. The lattice parameters of the $BaTiO_3$ sample were measured as $a = 3.998(6)$ Å in the cubic phase and $a = 3.983(6)$ Å and $c = 4.019(8)$ Å in the tetragonal phase at room temperature.

3. Data Evaluation

The crucial step in 3D-XRD data evaluation is the indexing, that is, identifying subsets of diffraction spots that belong to "individually diffracting domain structures". For ferroelectrics, an individually diffracting domain structure may consist of many layers within the grain (intercalated by layers belonging to different domain structures), where the misorientation between consecutive layers is small as compared to the instrumental orientation resolution (about 0.1°), while the cumulative misorientation may be larger than the orientation resolution. Such domain structures would result in smooth but broadened diffraction spots at room temperature. It was found that automated indexing software could not be successfully applied to the images recorded at room temperature. This is due to several compounding complications. First, due to the small tetragonal distortion the cubic reflections split into subreflections of which only the {2 0 0}/{0 0 2} and {2 1 1}/{1 1 2} were fully resolved radially by the detector resolution. Second, due to the large sample thickness-to-grain size ratio, the misorientations of domain structures within a grain are not negligible compared to the average azimuthal separation of (cubic) diffraction spots along the diffraction rings. Thus, clusters of diffraction spots that belong to a pseudocubic parent grain could not be identified. Finally, the diffraction spots of domain structures displayed an orientation spread resulting in partial spot overlap. Therefore, the room temperature diffraction patterns could not be indexed by automated algorithms. Instead, by heating above Curie temperature, a complete data set was recorded for cubic symmetry. Then, the sample

was slowly cooled down to room temperature, while data sets were acquired. The cubic data set was indexed with the automated GRAINDEX software [12], and the splitting of the cubic reflections due to the formation of tetragonal domains could be tracked from the data recorded during the cooling. Thus, clusters of diffraction spots belonging to domain structures of a cubic parent grain could be tracked to room temperature. Finally, these spots were assigned manually to domain structures by comparison to tetragonal lattice plane angles. This procedure is described in the following.

The GRAINDEX software first searches all individual images belonging to a data set for diffraction spots as defined by an intensity threshold and some topological criteria. Each spot is labeled with its $\{\theta, \phi, \eta\}$ angles (see Figure 1). From these angles, the reciprocal lattice vector of the diffracting lattice planes in the laboratory coordinate frame, G_l, is obtained as

$$G_l = \frac{4\pi \sin(\theta)}{\lambda} \cos(\theta) \begin{pmatrix} -\tan(\theta) \\ -\sin(\eta) \\ \cos(\eta) \end{pmatrix}, \tag{2}$$

where λ is the wavelength. The relation to the reciprocal hkl lattice vector in the sample coordinate system is given by

$$G_S = g^{-1} B \begin{pmatrix} h \\ k \\ l \end{pmatrix}, \tag{3}$$

$$G_l = \Phi G_s = \begin{pmatrix} \cos(\phi) & -\sin(\phi) & 0 \\ \sin(\phi) & \cos(\phi) & 0 \\ 0 & 0 & 1 \end{pmatrix} G_s. \tag{4}$$

The B matrix transforms the hkl reciprocal lattice vector into a Cartesian crystal coordinate system, and G_s is the reciprocal lattice vector in the sample coordinate system [12, 18]. GRAINDEX returns the orientation matrix g^{-1} of a grain if the completeness is above a set threshold value. The completeness is the ratio of the number of experimentally observed reflections divided by the number of expected reflections, assuming perfect spot finding and that the grain was perfectly centered on the rotation axis.

The manual assignment of diffraction spots to tetragonal domains of a parent grain was based on the analysis of orientation maps. The orientation maps are obtained by radial integration of a specific hkl diffraction ring. For one image, the result is a one-dimensional intensity distribution versus the η angle at the ϕ interval where the image was acquired. An orientation map is made up of the radially integrated η intensity profiles for all images of a ϕ rotation scan. Orientation maps provided an efficient visualization of the gradual splitting of cubic reflections into sets of tetragonal reflections from domain variants during cooling. The identification of spots belonging to domains of a common parent grain was furthermore confirmed by the analysis of sections of orientation maps around Friedel pair reflections (hkl) and $(\bar{h}\,\bar{k}\,\bar{l})$. The η angles of the respective scattering vectors G_l^{hkl} and $G_l^{\bar{h}\bar{k}\bar{l}}$ are separated by 180° and ϕ angles by at least 2θ (depending on η). Due to the inversion symmetry inherent to diffraction, these maps should be symmetric except for domains not centered on the rotation axis that may move in and out of the beam during the required ϕ rotation. While the ϕ rotations are typically only somewhat larger than 2θ, this rotation was often sufficient to move not centered domains at least partially in and out of the narrow beam. Thus, peaks that appear in Friedel pair orientation maps with unequal intensity are not close to the rotation axis and therefore not due to diffraction off domains from the centered reference grain.

The orientations of the tetragonal domain structures that originated from a cubic parent grain were obtained from {0 0 2} and {1 1 2} reflections since they are radially resolved and not subjected to overlap of equivalent reflections of 90° domains. Therefore, the η and ϕ coordinates of these reflections were obtained by fitting two-dimensional Gaussian distributions to the respective peaks in the orientation maps. The scattering angle θ was obtained from a "powder scan" which was produced by adding all diffraction images of an indexing scan and azimuthal integration over η. The $\{\theta, \phi, \eta\}$ angles were then transformed to scattering vectors in the sample frame, G_s, using (2) and (4). The scattering vectors for {0 0 2} and {1 1 2} that belong to the same domain family were identified by the angle between the measured scattering vectors as compared to the theoretical angle for a tetragonal unit cell, given by

$$\cos(\psi) = \frac{(h_1 h_2 + k_1 k_2)/a^2 + l_1 l_2 / c^2}{\sqrt{(h_1^2 + k_1^2)/a^2 + (l_1^2/c^2)}\sqrt{(h_2^2 + k_2^2)/a^2 + (l_2^2/c^2)}}. \tag{5}$$

The orientation matrix g^{-1} was then obtained by least-squares optimization of (3). The orientations were validated by simulating the complete diffraction patterns and comparison to the experimental orientation maps [12]. The deviations were within 0.1° in ϕ and 0.05° in η. The crystallographic orientations were represented as orientation matrices mapped into the fundamental regions for the respective cubic or tetragonal symmetry. The misorientations were presented in angle-axis notation [21, 22] and were calculated by the ODF/PF software package from Cornell University [23].

4. Results and Discussion

The Curie temperature, at which the cubic-tetragonal phase transformation takes place, was measured as 125.3 ± 0.1°C [24] from capacitance versus temperature measurements with a separate $BaTiO_3$ sample made from the same processing batch. We first discuss the phase transformation by analyzing diffraction patterns as observed directly on the detector. Information is obtained along the radial (2θ) and one azimuthal direction (η). Regions of interest (ROI) are selected around the cubic {200} reflections and several adjacent ϕ-frames are summed achieving proper integration in this azimuthal direction. The resulting plots are shown in Figure 2.

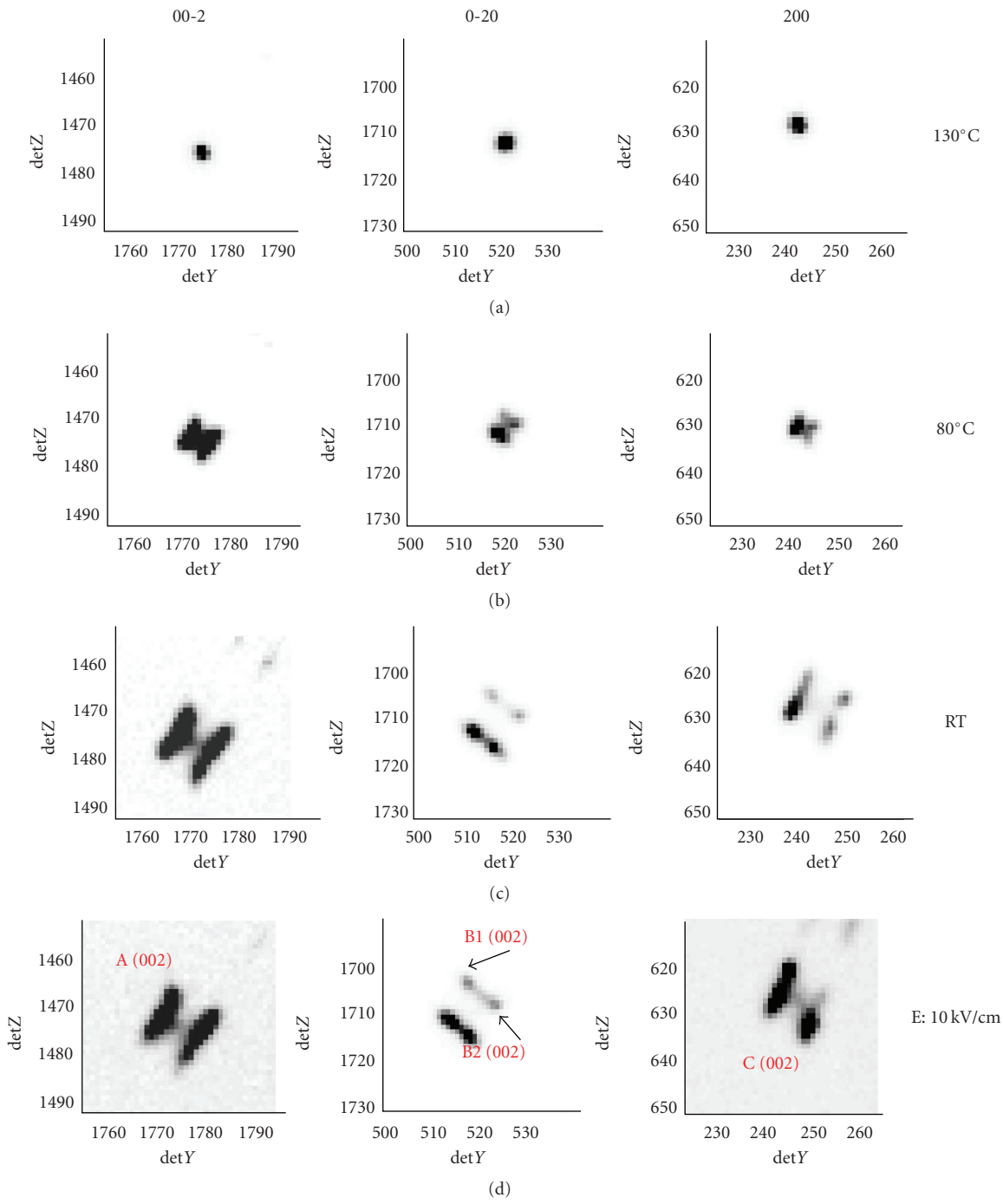

Figure 2: The evolution of (002) and (200) peaks during cooling to room temperature and after applying an electric field of 10 kV/cm at room temperature (last row). The four spots at room temperature that represent the domain structures are indicated.

A gradually increasing radial peak splitting is obvious during cooling, when the cubic phase ($Pm\bar{3}m$) transforms to a tetragonal phase (P4 mm). It is also seen that tetragonal *a*- and *c*-axes reflections appear at similar η-angles which is consistent with the cubic unit cell slightly contracting along the *a* axis and expanding along the *c* axis [25], without major orientation changes. The widths of the {002} reflections in radial and η-direction were evaluated from the appropriate projections after transformation to polar coordinates and are compiled in Table 1.

A significant peak broadening was observed along the azimuthal η-direction at room temperature. The full width half maximum (FWHM) of the peaks along the azimuthal η-direction was calculated as $0.1 \pm 0.01^\circ$ at above Curie temperature and $0.29 \pm 0.08^\circ$ at room temperature. The peak broadening along η can be well detected by the technique

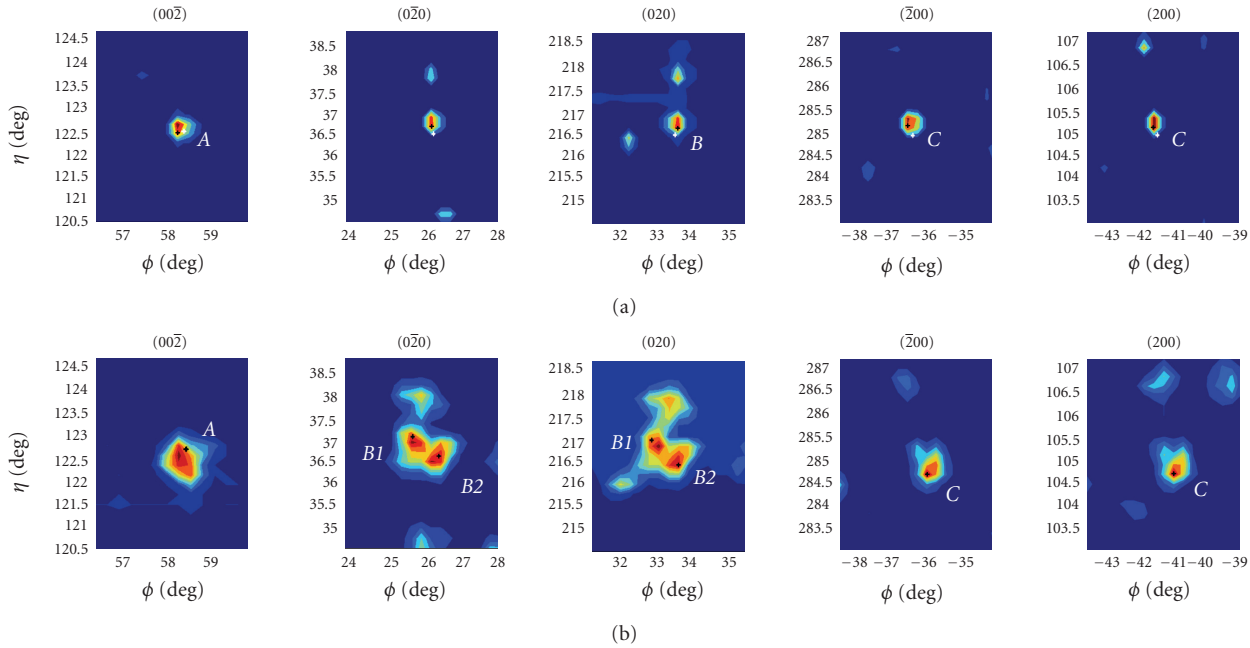

Figure 3: The ϕ-η distribution of {200} peaks of the reference grain above the Curie temperature (a) and (002) peaks of the domains at room temperature (b). The markers (+) represent the orientations shown in Table 2. The figures with opposite *hkl* signs and a similar pattern are from Friedel pairs of the same reflections.

Table 1: Widths of the {002} peaks along radial (2θ) and azimuthal (η) direction at 130°C and room temperature.

Domain	*A*		*B*1		*B*2		*C*	
	130°C	RT	130°C	RT	130°C	RT	130°C	RT
2θ, FWHM, pixel	1.81	2.29	2.24	2.45	2.25	2.45	1.63	2.22
2θ, FWHM, °	0.01	0.014	0.012	0.015	0.01	0.012	0.01	0.015
η, FWHM, pixel	1.52	5.7	1.65	4.28	1.65	3.63	1.36	3.37
η, FWHM, °	0.10	0.37	0.108	0.28	0.108	0.24	0.09	0.22

since the resolution along η is 0.04°. Along the radial direction, the average FWHM of the peaks was measured as $0.011 \pm 0.001°$ at 130°C and $0.014 \pm 0.002°$ at room temperature. While the measured radial broadening is small, it must be taken into account that the radial peak width above Curie temperature is dominated by the detector resolution and the measured broadening, therefore, is only a lower limit of the real broadening. Both the radial and azimuthal broadening are considered as evidence of inter- and intragranular constrains effecting the phase transformation.

In the following, a detailed discussion of the mutual misorientations of the observed four domain structures is presented. As described in Section 3, the precise domain orientations were obtained by manual evaluation of ϕ-η orientation maps. Figure 3 shows the respective sections for the (002) reflections. Good agreement is evident between predicted and observed peak positions. As discussed in Section 3, several close-by peaks are identified as not belonging to the reference grain from the Friedel pair analysis. Again, the azimuthal peak broadening at room temperature is obvious.

Table 2 shows the orientations of the domain structures at room temperature and of the cubic grain above the Curie temperature, presented as orientation matrices g^{-1}. Domain misorientations are presented for two models discussed below. The listed *c*/*a* ratios were evaluated from the radial positions of the respective {200} and {002} reflections.

The first model assumes the tetragonal domains to be mutually orthogonal and related by 90° rotations around ⟨100⟩ directions. An arbitrary misorientation is allowed against the cubic grain. The selection of domain *A* as reference is arbitrary for the 90° model but any other selection results in similar misorientations. The misorientations are significant compared to the experimental accuracy of 0.1°. Furthermore, the observed splitting of domain structures *B*1 and *B*2 cannot be explained.

The second model is based on twinning on {101} habit planes, as sketched in Figure 4. A small distortion angle $\alpha = 90° - \gamma$ results between the *a*- and *c*-axes dependent on the *c*/*a* ratio as given by (1). In addition to the parent domain four twin domains result which can be divided into two pairs with a small internal misorientation of 2α around a ⟨100⟩

Table 2: Orientations of the four identified domain structures and of the cubic grain above Curie temperature. Also listed are the misorientations between the domain structures and two models (for discussion see text). Finally, the c/a ratios are listed as experimentally determined from the {0 0 2} and {2 0 0} lattice spacings.

	Orientation	Orientation matrix			Misorientation for 90° rotations around ⟨100⟩	Misorientation for tetragonal twins	Habit plane	c/a ratio
Room temperature	A	0.60705	0.29543	0.73770	Reference	Reference	Parent	1.0092
		−0.75016	0.51935	0.40932				
		−0.26220	−0.80187	0.53689				
	$B1$	0.74107	−0.60357	−0.29414	0.29°	0.50°	(011)	1.0093
		0.40680	0.75214	−0.51847				
		0.53417	0.26456	0.80292				
	$B2$	0.73815	−0.60403	−0.30047	0.43°	0.27°	$(0\bar{1}1)$	1.0093
		0.40309	0.75202	−0.52152				
		0.54098	0.26384	0.79858				
	C	0.74035	0.29485	−0.60411	0.27°	0.28°	(101)	1.0091
		0.40577	0.52048	0.75130				
		0.53594	−0.80136	0.26569				
$T > T_C$ (130°C)	D	0.60572	0.30001	0.73695	0.32°	n/a	n/a	1
		−0.75272	0.51627	0.40852				
		−0.25790	−0.80216	0.53853				

direction. Domains belonging to a pair are referred to as domain variants.

The twinning model provides a qualitative explanation of the observed splitting of the $B1$ and $B2$ domains as domain variants. Quantitatively, the misorientation axis closely agrees with an a-axis of the A-domain but the splitting is only half the expected value from the c/a ratio. Nevertheless, the A-domain is the only natural choice for the parent domain. The misorientations between the measured domain orientations and the model predictions are found from Table 2 to be about 0.3°. Again, this is significant as compared to the experimental accuracy of 0.1° and as compared to the α angle of 0.52°. Thus, the misorientations cannot be caused by variations of the c/a ratio. We also note that the misorientations could not be significantly reduced by fitting an arbitrary c/a ratio. Finally, it is noted that only one variant of the C-domains was observed experimentally. Figure 5 visualizes the domain orientations in pole figures.

We conclude that neither the 90° rotation model around ⟨100⟩ directions nor the twinning model on {101} habit planes is in quantitative agreement with the experiment and suggest that the misorientations are due to locally varying intra- and intergranular constrains. Proof of this conclusion would require the evaluation of domain misorientations from a statistically significant number of grains. The methodology presented here could provide such data sets if the evaluation can be automated.

After cooling to room temperature, an electric field was applied to the sample up to 10 kV/cm. Since the coercive field of $BaTiO_3$ was measured as 5.14 kV/cm with polarization versus temperature measurements; the applied electric field was enough for texture development and to trigger domain reorientation. First, the macroscopic response was investigated by monitoring the intensity of (002) reflections with scattering vectors parallel to the applied electric field. Domain reorientation during the applied field was studied by integrating oscillation diffraction images within a range of

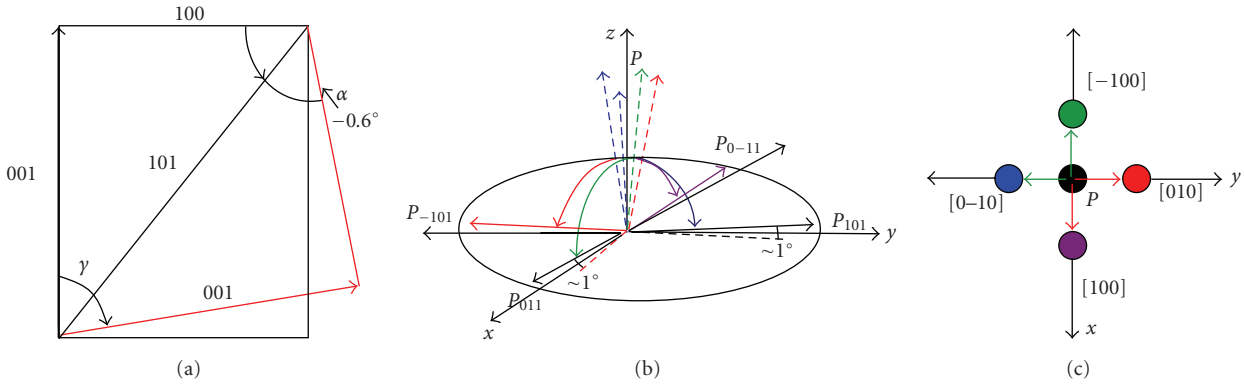

FIGURE 4: (a) Schematic representation of the twinning operation on {101} habit planes. The *c*/*a* ratio is exaggerated for clarity. (b) Schematic representation of the polarization directions of the four twin domains. (c) Projection along the *z* direction of the parent showing the four ⟨100⟩ twin orientations. The angle between two domain variants corresponds to 1.049° when the *c*/*a* ratio is taken as 1.0092.

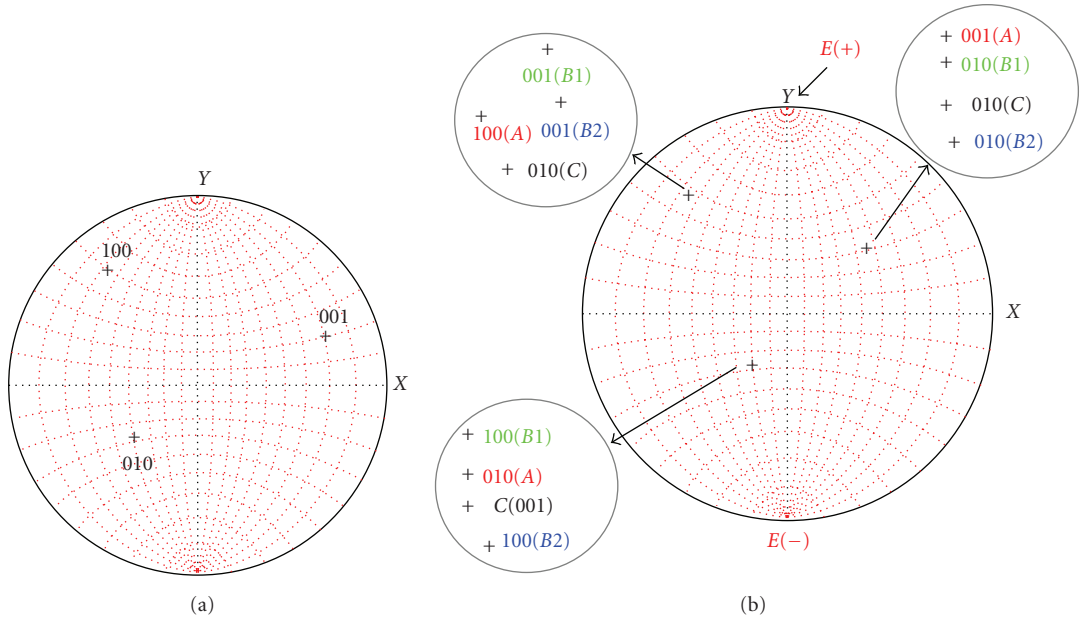

FIGURE 5: (a) 100 pole figure of the grain at a temperature above the Curie temperature. *XYZ* coordinates refer to directions of sample coordinate system used in the experiment. (b) 001 pole figure of the ferroelectric domain orientations at room temperature. A Wulff net is overlaid for clarity. The orientations correspond to those presented in Table 2.

$\pm 60°$ in ϕ and parallel to the electric field (η: $90° \pm 5°$) using the *Fit2D.v12.077* software [19]. The multiple of a random distribution (mrd) of the reflections are calculated from the integrated intensities of the reflections shown in Figure 2

$$f_{002}\,[\text{mrd}] = 3 \cdot \frac{I_{002}/I_{002}^{\text{unpoled}}}{I_{002}/I_{002}^{\text{unpoled}} + 2 \cdot \left(I_{200}/I_{200}^{\text{unpoled}}\right)}, \quad (6)$$

where I_{hkl} is the integrated intensity of *hkl* spots. While f_{002} was 1 prior to the applied electric field which represents a randomly oriented domain structure, the mrd value increased to 1.65 with the applied electric field. The mrd values show that the crystals in the sample experienced a significant change of volume fraction associated to domain wall migration under electric field.

Next, we turn to the individual domains of the reference grain. The orientations of the domains were evaluated at 0, 5, and 10 kV/cm applied electric field. Figure 6 shows the misorientations of the individual domains against the orientations at 0 applied field. Within the 0.1° experimental accuracy, no significant orientation changes were observed.

With the application of the electric field, the domains with the smallest polarization angle to the electric field are expected to grow. The domain walls move in response

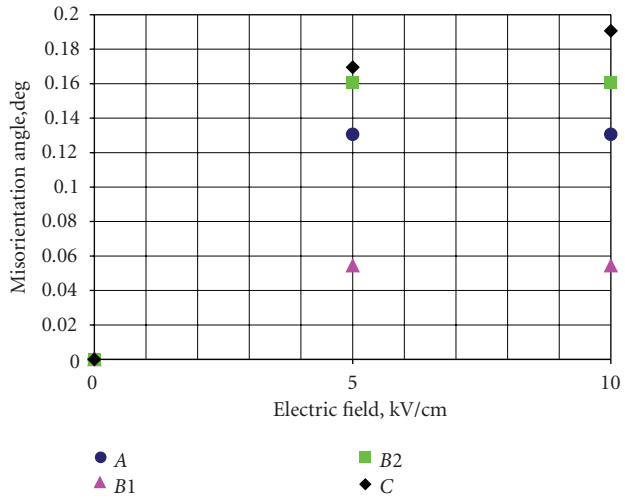

Figure 6: Domain misorientations as function of the applied electric field.

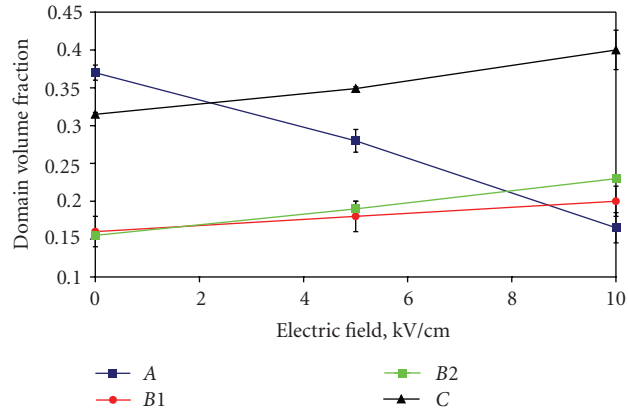

Figure 7: Volume fraction change of the domain structures with applied electric field. The error bars show the uncertainties from independent measurements of the Friedel pairs.

to electric field, and the volume fraction of the most energetically favorable domain or domains will increase. To predict which domain should grow with the electric field, the angle between the c axis of the domain and the electric field direction was calculated from the orientation matrices of the domains. We define this angle as the "polarization angle". The polarization angles for domains A, $B1$, $B2$, and C were calculated as 65.8°, 58.8°, 58.6, and 41.3°, respectively. Since domain A has a large polarization angle, the volume fraction of this domain in the grain is expected to decrease with the application of electric field.

There is a direct relation between the volume of a domain structure and the integrated intensity [26]. In order to observe the volume fraction change between domain variants with applied electric field, the integrated intensities of the domains were evaluated and the volume fraction of the domains inside the grain (f^d_{002}) was calculated by using (6). The reflections were taken from the domain variants shown in Figure 3. To eliminate the effect of the Lorentz factor, the domain structures that diffract at the same η and ϕ were taken. For instance, the (002) reflection of domain A diffracting at $\eta = 122.5°$ and $\phi = 58.4°$ is compared with the (200) and (020) reflections of domains $B1$, $B2$, and C at the same η and ϕ. For many cases, the integrated intensities of (200) and (020) reflections of domain variants were difficult to resolve due to spot overlap and the sum of these overlapped spots were taken in the calculation. To improve the statistics, the Friedel pairs of each spot were measured as well.

Figure 7 shows the volume fraction change in the domain structures with applied electric field. The volume fraction of domain C increases with increasing electric field as expected by its small polarization angle. With its high-polarization angle, the volume fraction of domain A decreases by around 50%. The volume fractions of domains $B1$ and $B2$ increase with electric field as well, but this increase is not as significant as that of domain C. The systematic dependence of the volume fractions with applied electric field upon the polarization angles is proof of 90° domain switching.

5. Conclusions

The orientations and volume fractions of ferroelectric domains within a polycrystalline $BaTiO_3$ sample were investigated by the 3D-XRD technique during cooling from the cubic phase to room temperature and subsequently as function of an applied electric field. The technique enables the *in situ* observation of true bulk grains, at the center of 1 mm thick sample.

While the recorded datasets contain information on several grains, here, only results from a selected reference grain are presented due to the lack of automated evaluation software. The assignment of diffraction spots to tetragonal domain structures is challenging as the spot density is high, individual spots exhibit significant orientation spread, and most *hkl* multiplets are not resolved radially within the detector resolution. These difficulties were overcome by following the evolution of diffraction spots while cooling the sample from above Curie temperature and by a manual analysis of the identified diffraction spots from individual domain structures.

It was found that while the orientation spread of the cubic grains is below the instrumental resolution, the tetragonal domain structures exhibited an azimuthal orientation spread of about $0.3 \pm 0.05°$ FWHM at room temperature. For the reference grain, three almost orthogonal domain structures were present and found to be misoriented by about 0.3° in respect to the cubic grain of origin. One of the domain structures split into two peaks of about 0.48° misorientation.

The achieved orientation resolution of 0.1° enables a decisive quantitative test of models describing the domain formation. It is found that neither 90° rotations about ⟨100⟩ axes nor twinning on {101} habit planes are in quantitative agreement to measured domain orientations. The remaining misorientations of about 0.3° are a significant fraction of the c/a ratio dependent distortion angle $\alpha = 0.5°$ due to twinning on {101} habit planes. It is suggested that local intra- and intergranular constrains produce misorientations of the observed magnitude. The presented experimental

methodology can provide data on a large number of grains but automated data evaluation would be required.

Upon application of an electric field, the volume fractions of the domain structures changed systematically favoring growth of domain structures with small polarization angle. This finding is proof for 90° domain switching. No significant rotation of domain structures was observed upon application of an electric field which is consistent with domain boundary migration.

Acknowledgments

3D-XRD data was collected at the X-ray Operations and Research beamline 1-ID-C at the Advanced Photon Source, Argonne National Laboratory. Use of the Advanced Photon Source at Argonne National Laboratory was supported by the US Department of Energy, Office of Science, Office of Basic Energy Sciences, under Contract no. DE-AC02-06CH11357. The authors would like to thank Dr. Jon Almer, Ali Mashayekhi from APS, Dr. Joel Bernier from LBNL, and Allan Lyckegaard from Risø for their help in the experiments and Drs. Dean Haeffner and Brian H. Toby from APS and Dr. Wolfgang Pantleon from Risø for helpful discussions.

References

[1] F. Jona and G. Shirane, *Ferroelectric Crystals*, Pergamon Press, Oxford, UK, 1962.

[2] B. Jaffe, *Piezoelectric Ceramics*, Academic Press, London, UK, 1971.

[3] G. H. Haertling, "Ferroelectric ceramics: history and technology," *Journal of the American Ceramic Society*, vol. 82, no. 4, pp. 797–818, 1999.

[4] M. E. Lines and A. M. Glass, *Principles and Applications of Ferroelectrics and Related Materials*, Clarendon Press, Oxford, UK, 1977.

[5] G. Arlt, "Twinning in ferroelectric and ferroelastic ceramics: stress relief," *Journal of Materials Science*, vol. 25, no. 6, pp. 2655–2666, 1990.

[6] X. Tan and J. K. Shang, "Intersection of a domains in the c-domain matrix driven by electric field in tetragonal ferroelectric crystal," *Journal of Applied Physics*, vol. 96, no. 5, pp. 2805–2810, 2004.

[7] K. A. Schönau, M. Knapp, H. Kungl, M. J. Hoffmann, and H. Fuess, "In situ synchrotron diffraction investigation of morphotropic $Pb[Zr_{1-x}Ti_x]O_3$ under an applied electric field," *Physical Review B*, vol. 76, no. 14, Article ID 144112, 2007.

[8] X. R. Huang, S. S. Jiang, W. J. Liu et al., "Contrast of ferroelastic and ferroelectric domains in white-beam X-ray topographs," *Journal of Applied Crystallography*, vol. 29, pp. 371–377, 1996.

[9] F. Ernst, M. L. Mulvihill, O. Kienzle, and M. Rühle, "Preferred grain orientation relationships in sintered perovskite ceramics," *Journal of the American Ceramic Society*, vol. 84, no. 8, pp. 1885–1890, 2001.

[10] S. Balakumar, J. B. Xu, J. X. Ma, S. Ganesamoorthy, and I. H. Wilson, "Surface morphology of ferroelectric domains in $BaTiO_3$ single crystals: an atomic force microscope study," *Japanese Journal of Applied Physics*, vol. 36, no. 9, pp. 5566–5569, 1997.

[11] S. V. Kalinin and D. A. Bonnell, "Temperature dependence of polarization and charge dynamics on the $BaTiO_3(100)$ surface by scanning probe microscopy," *Applied Physics Letters*, vol. 78, no. 8, pp. 1116–1118, 2001.

[12] E. M. Lauridsen, S. Schmidt, R. M. Suter, and H. F. Poulsen, "Tracking: a method for structural characterization of grains in powders or polycrystals," *Journal of Applied Crystallography*, vol. 34, no. 6, pp. 744–750, 2001.

[13] H. F. Poulsen, J. R. Bowen, and C. Gundlach, "Characterising the dynamics of individual embedded dislocation structures," *Scripta Materialia*, vol. 51, no. 8, pp. 783–788, 2004.

[14] L. Margulies, G. Winther, and H. F. Poulsen, "In situ measurement of grain rotation during deformation of polycrystals," *Science*, vol. 291, no. 5512, pp. 2392–2394, 2001.

[15] T. A. Byrne and D. P. Cann, "Effects of silver on barium titanate as a function of stoichiometry," *Journal of the American Ceramic Society*, vol. 87, no. 5, pp. 875–880, 2004.

[16] J. H. Lee, C. C. Aydiner, J. Almer et al., "Synchrotron applications of an amorphous silicon flat-panel detector," *Journal of Synchrotron Radiation*, vol. 15, no. 5, pp. 477–488, 2008.

[17] M. Varlioglu, *Mesoscale Constitutive Behavior of Ferroelectrics*, Ph.D. thesis, Iowa State University, 2009.

[18] H. F. Poulsen, *Three-Dimensional X-Ray Diffraction Microscopy: Mapping Polycrystals and Their Dynamics*, Springer, New York, NY, USA, 2004.

[19] A. P. Hammersley, "ESRF Internal Report," ESRF97HA02T, 1997.

[20] B. D. Cullity and S. R. Stock, *Elements of X-Ray Diffraction*, Prentice Hall, Upper Saddle River, NJ, USA, 3rd edition, 2001.

[21] F. C. Frank, "Orientation mapping," *Metallurgical Transactions A*, vol. 19, no. 3, pp. 403–408, 1988.

[22] A. Morawiec, "Distributions of misorientation angles and misorientation axes for crystallites with different symmetries," *Acta Crystallographica Section A*, vol. 53, no. 3, pp. 273–285, 1997.

[23] P. Dawson, D. Boyce et al., "The DPLAB Polycrystal Library at Cornell," http://anisotropy.mae.cornell.edu/.

[24] M. Varlioglu, E. Ustundag, N. Tamura, and J. L. Jones, "Evolution of ferroelectric domain structures embedded inside polycrystalline $BaTiO_3$ during heating," *Journal of Applied Physics*, vol. 107, no. 6, Article ID 064101, 2010.

[25] R. H. Buttner and E. N. Maslen, "Structural parameters and electron density in $BaTiO_3$," *Acta Crystallographica Section B*, vol. 48, no. 6, pp. 764–769, 1992.

[26] E. C. Subbarao, M. C. McQuarrie, and W. R. Buessem, "Domain effects in polycrystalline barium titanate," *Journal of Applied Physics*, vol. 28, no. 10, pp. 1194–1200, 1957.